

Article

# Advanced Ga<sub>2</sub>O<sub>3</sub>/Lignin and ZrO<sub>2</sub>/Lignin Hybrid Microplatforms for Glucose Oxidase Immobilization: Evaluation of Biosensing Properties by Catalytic Glucose Oxidation

Artur Jędrzak<sup>1</sup>, Tomasz Rębiś<sup>2</sup>, Maria Kuznowicz<sup>1</sup>, Agnieszka Kołodziejczak-Radzimska<sup>1</sup>, Jakub Zdarta<sup>1</sup> , Adam Piasecki<sup>3</sup>  and Teofil Jesionowski<sup>1,\*</sup> 

<sup>1</sup> Institute of Chemical Technology and Engineering, Faculty of Chemical Technology, Poznan University of Technology, Berdychowo 4, PL-60965 Poznan, Poland; artur.f.jedrzak@doctorate.put.poznan.pl (A.J.); maria.m.kuznowicz@doctorate.put.poznan.pl (M.K.); agnieszka.kolodziejczak-radzimska@put.poznan.pl (A.K.-R.); jakub.zdarta@put.poznan.pl (J.Z.)

<sup>2</sup> Institute of Chemistry and Technical Electrochemistry, Faculty of Chemical Technology, Poznan University of Technology, Berdychowo 4, PL-60965 Poznan, Poland; tomasz.rebis@put.poznan.pl

<sup>3</sup> Institute of Materials Science and Engineering, Faculty of Mechanical Engineering and Management, Poznan University of Technology, Jana Pawła II 24, PL-60965 Poznan, Poland; adam.piasecki@put.poznan.pl

\* Correspondence: teofil.jesionowski@put.poznan.pl

Received: 30 October 2019; Accepted: 4 December 2019; Published: 9 December 2019



**Abstract:** In this study, novel Ga<sub>2</sub>O<sub>3</sub>/lignin and ZrO<sub>2</sub>/lignin hybrid materials were obtained and used as supports for the adsorption of the enzyme glucose oxidase (GOx). A biosensor system based on the hybrid supports was then designed to determine the concentration of glucose in various solutions. The obtained bioinspired platforms were analyzed to determine chemical and physical properties of the support structures. A determination was made of the effectiveness of the proposed method of immobilization and the quality of operation of the constructed glucose biosensor in electrochemical tests. To characterize the materials, Fourier transform infrared spectroscopy (FT-IR), transmission electron microscopy (TEM), scanning electron microscopy (SEM), X-ray diffraction (XRD), thermogravimetric analysis (TGA), electrokinetic (zeta) potential measurements, atomic force microscopy (AFM), particle size measurements (NIBS technique), and elemental analysis (EA) were used. In further research, glucose oxidase (GOx) was immobilized on the surface of the obtained functional Ga<sub>2</sub>O<sub>3</sub>/lignin and ZrO<sub>2</sub>/lignin biomaterials. The best immobilization capacities—24.7 and 27.1 mg g<sup>-1</sup> for Ga<sub>2</sub>O<sub>3</sub>/lignin and ZrO<sub>2</sub>/lignin, respectively—were achieved after a 24 h immobilization process. The Ga<sub>2</sub>O<sub>3</sub>/Lig/GOx and ZrO<sub>2</sub>/Lig/GOx systems were used for the construction of electrochemical biosensor systems, in a dedicated carbon paste electrode (CPE) with the addition of graphite and ferrocene.

**Keywords:** gallium oxide; zirconium dioxide; (bio)hybrid; glucose oxidase; enzyme immobilization; biosensor

## 1. Introduction

Hybrid materials have existed on Earth for millions of years. There are many examples of combinations of inorganic and organic components that occur in nature, including shells of mollusks and components of human bones [1–5]. Over time, people took notice that combinations of two or more components could enable the fabrication of a material with new properties that were not exhibited by the separate components. This was just the beginning, as the new properties of hybrid connections are still being explored and their potential has not yet been fully exploited [2–6]. Hybrid materials

are most often defined as systems consisting of a homogeneous mixture of inorganic and organic components that are mixed together at the molecular level. This structural limitation means that the resulting products offer specific properties that the original components do not possess. The wide range of possibilities of designing the composition of hybrid materials means they have huge potential for application in many fields of science and industry [5–9].

Lignin is the second most abundant natural polymer with amorphous character. It is an attractive component due to the rich aromatic character of the biopolymer [3–5]. This is responsible for its high affinity to carbon-based materials, in addition to strong adsorption on the  $sp^2$ -hybridized carbon surfaces of platforms [10–12].

An immobilization is a process of confining cell, enzymes, or other biomaterials on special inert and insoluble matrix. There are several methods of immobilization, and depending on the method chosen, the binding of the biocatalyst may occur more or less permanently. This technique is used to improve the properties of biocatalysts and the efficiency of catalytic processes while reducing process costs. [13–16]. Immobilization prevents the loss of catalytic activity, which allows multiple use of produced biocatalytic systems. The separation of immobilized biosystems from the reaction process is easier and faster, making them more attractive for industrial applications [13,16,17]. Immobilization processes are of great significance in many branches of industry, including the chemical, pharmaceutical, and biological sectors. Additionally, the possibility of enzyme immobilization may contribute to the ongoing progress in bioprocesses and in biosensing [5].

Over the years, glucose oxidase (GOx) has been increasingly used in the construction of biosensor systems [18–20]. Glucose oxidase is a flavoprotein that catalyzes the oxidation of  $\beta$ -D-glucose [18,21]. Many commercially available glucose sensors are based on immobilized glucose oxidase or glucose dehydrogenase, and they are particularly widely used in the food industry and medicine [18,21].

Today, metal oxide-based materials ( $ZrO_2$ ,  $Ga_2O_3$ ,  $CeO_2$ ,  $ZnO$ ,  $SiO_2$ ) are intensively studied as sophisticated supports for enzyme immobilization. This is due to their nontoxicity, biostability, biocompatibility, and ease of process separation [22,23]. Novel metal oxide-based platforms, like those using  $Ga_2O_3$  [24–28] or  $ZrO_2$  [29–34], provide better electron conductivity, a higher isoelectric point, and improved biocompatibility or bioactivity [35]. Wang and co-authors prepared humidity sensors based on  $Ga_2O_3$  which has satisfying sensing properties [24]. In addition, the use of thin layers of  $ZnO$  causes good electrical transport, high isoelectric point and cost effectiveness. Marie and co-workers investigated a glucose electrochemical sensor based on  $ZnO$  nanorods [36]. On the other hand, enzymatic glucose biosensor based on  $CeO_2$  was proposed by Patil and co-authors. They used cerium (IV) oxide because of electrical conductivity, biocompatibility, high specific surface area, and chemical inertness [37]. In their research, Golikova and co-workers immobilized the enzyme on the  $SiO_2$  and  $Al_2O_3$  surface. The advanced layout allows for effective immobilization and high activity and stability of biocatalysts [38].

The aim of this work was to obtain innovative hybrid biomaterials conforming to the principles of sustainable chemistry due to the use of by-products such as lignin in the microplatforms. The work consisted of several stages. First, modified zirconium dioxide and gallium oxide were attached separately to lignin [7]. Next, the glucose oxidase enzyme was immobilized on them by adsorption. A biosensor was constructed with a dedicated carbon paste electrode (CPE) to examine glucose solutions. Physicochemical analyses were carried out to enable the precise characterization of the obtained micromaterials.

## 2. Results and Discussion

### 2.1. Surface Morphology

The techniques that were used to determine the morphological structure of oxides and the obtained hybrid materials were transmission electron microscopy (TEM), scanning electron spectroscopy (SEM),

energy-dispersive X-ray spectroscopy (EDS), and X-ray diffraction analysis (XRD). The results of transmission electron microscopy are shown in Figure 1.

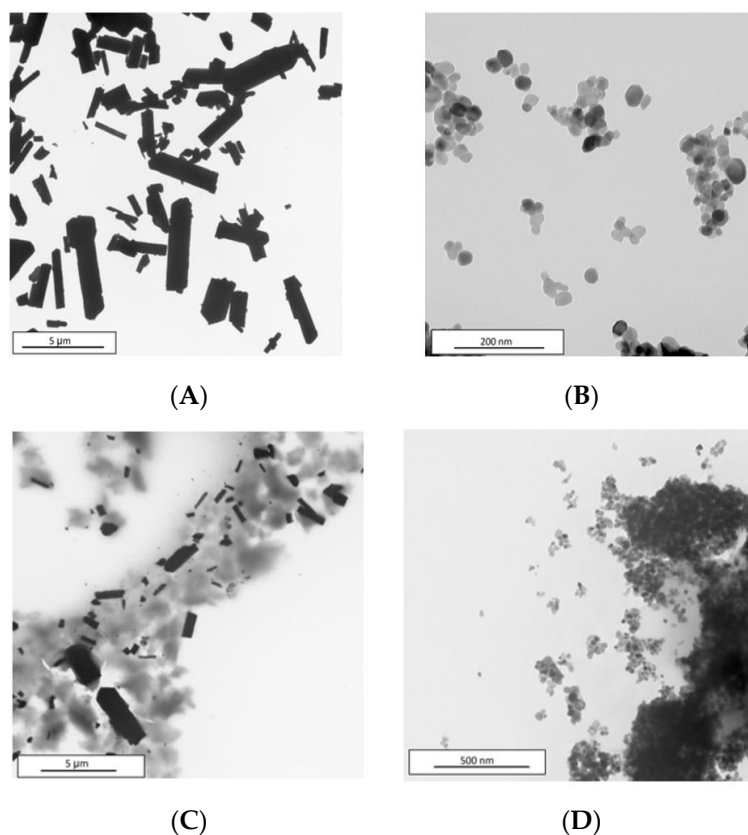


**Figure 1.** TEM micrographs of Ga<sub>2</sub>O<sub>3</sub> (A), ZrO<sub>2</sub> (B), Ga<sub>2</sub>O<sub>3</sub>/lignin (C), and ZrO<sub>2</sub>/lignin (D).

The bare Ga<sub>2</sub>O<sub>3</sub> particles have sizes ranging from 1 to 5 μm (Figure 1A). The micrograph of ZrO<sub>2</sub> presents spherical nanoparticles from 20 to 50 nm (Figure 1B). Both images show individual primary particles that tend to agglomerate to form larger clusters. The Ga<sub>2</sub>O<sub>3</sub>/lignin and ZrO<sub>2</sub>/lignin hybrid materials are shown in Figure 1C,D, respectively. The change in the morphology of the material, including the size of the repeated pattern observed in the TEM image, indirectly demonstrates the effectiveness of the combination of APTES-modified metal oxides with activated lignin. Scanning electron microscopy (SEM) was also used to determine the morphology of the components and the obtained hybrid materials (Figure 2).

The SEM micrographs present structures of Ga<sub>2</sub>O<sub>3</sub>, ZrO<sub>2</sub>, Ga<sub>2</sub>O<sub>3</sub>/lignin and ZrO<sub>2</sub>/lignin in a range of about 2–50 μm with the occurrence of irregularly shaped particles. It may be assumed from the shape and size of the particles that the materials will have a relatively small specific surface area and mainly macroscopic pores. The primary microparticles are capable of forming aggregates and agglomerates. The lignin component of the hybrid materials is visible. In the SEM micrographs of the resulting supports, stable irregularly shaped modules of modified gallium oxide or zirconium dioxide and activated lignin have merged together to form clusters of aggregates with no precisely outlined contours.

Energy Dispersive Spectroscopy (EDS) was used for the elements distribution analysis and mapping. The test was carried out for both pristine oxides (ZrO<sub>2</sub>, Ga<sub>2</sub>O<sub>3</sub>) and for hybrid supports (ZrO<sub>2</sub>/Lig, Ga<sub>2</sub>O<sub>3</sub>/Lig). The obtained results are presented in Figures 3–6.

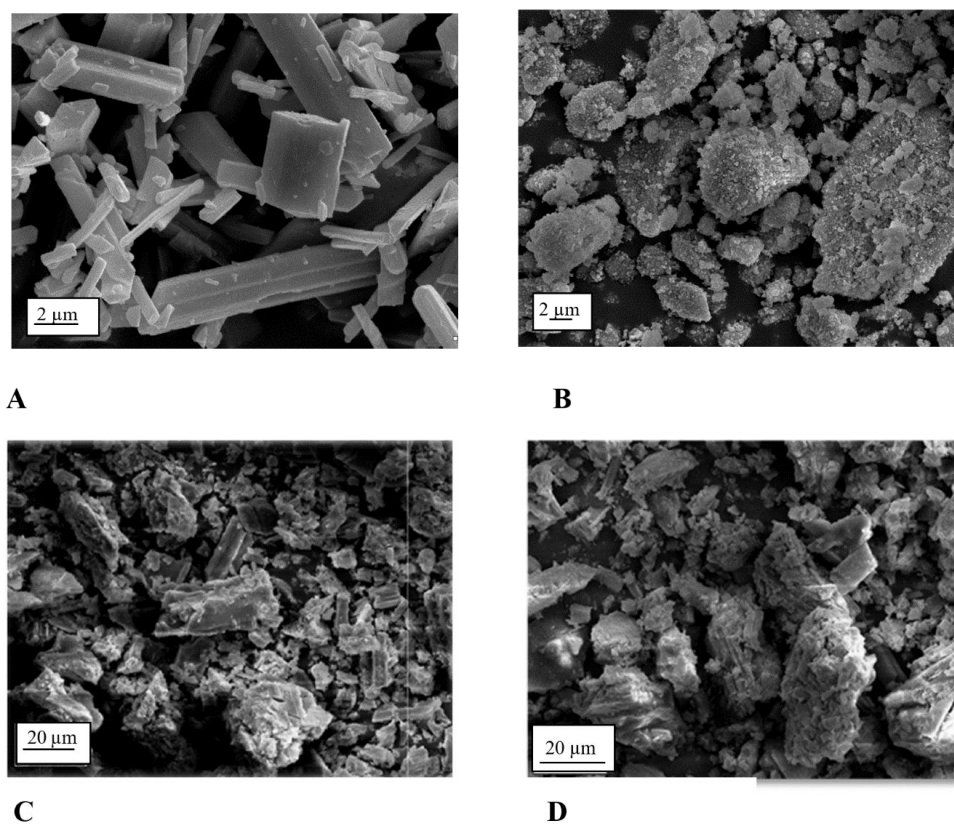


Figure 2. SEM micrographs: Ga<sub>2</sub>O<sub>3</sub> (A), ZrO<sub>2</sub> (B), Ga<sub>2</sub>O<sub>3</sub>/lignin (C), and ZrO<sub>2</sub>/lignin (D) supports.

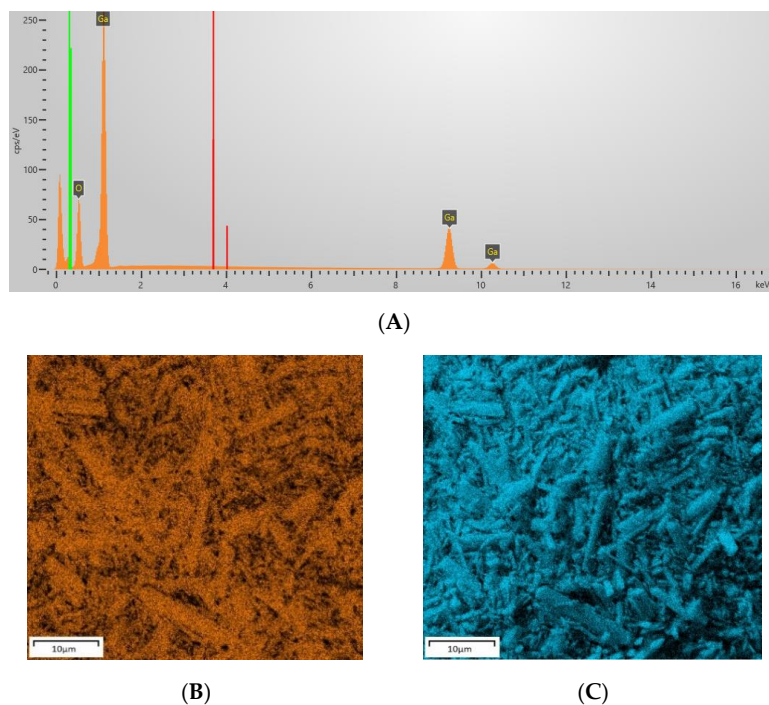
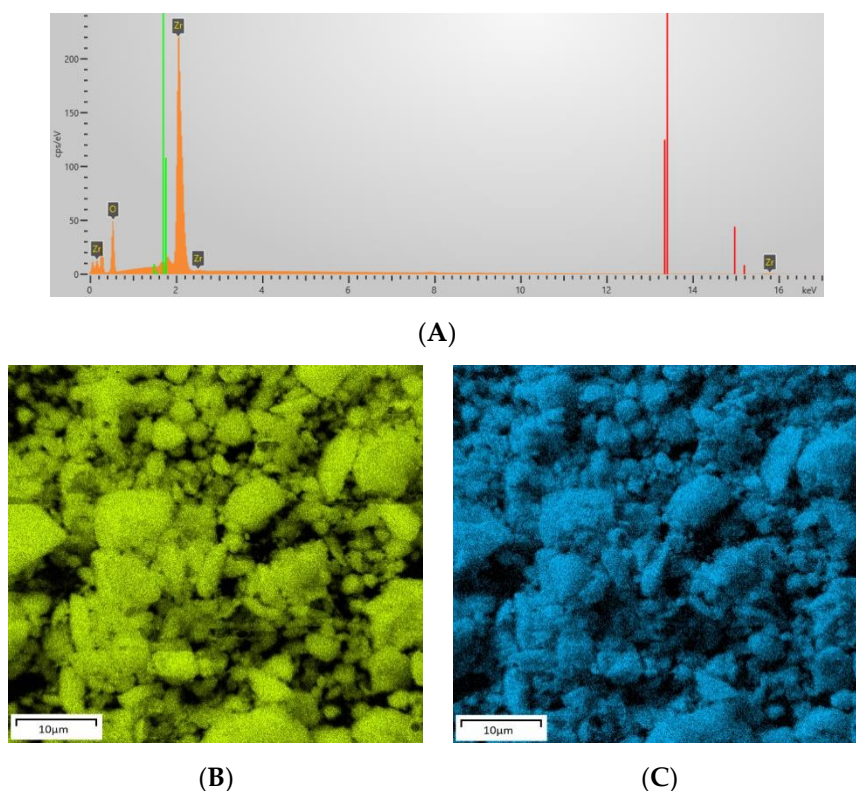
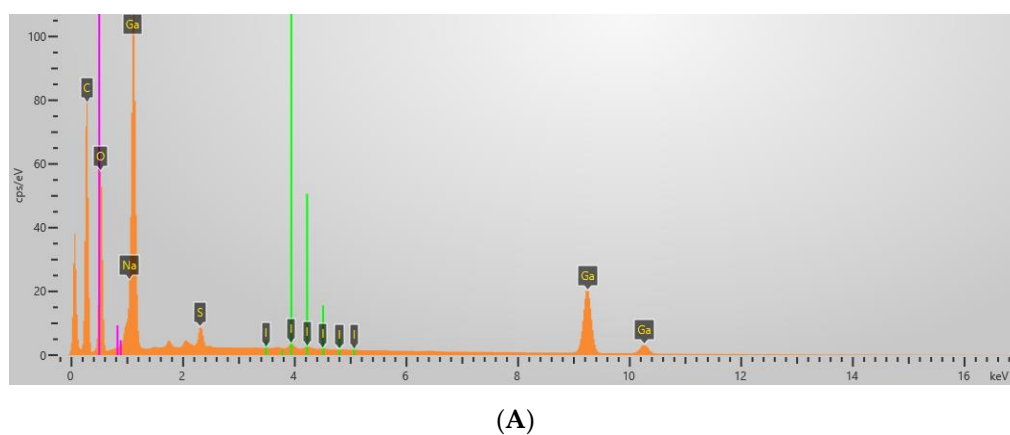


Figure 3. EDS mapping spectrum of Ga<sub>2</sub>O<sub>3</sub> (A) and SEM-micrographs of elemental gallium (B), oxygen (C).



**Figure 4.** EDS mapping spectrum of  $ZrO_2$  (A) and SEM-micrographs of elemental zirconium (B), oxygen (C).

The results of EDS also allowed the determination of the percentage content of elements (Ga, Zr, O, C, S, Na, and I). According to the EDS results, a strong peak from C and S are presented in  $Ga_2O_3/Lig$  and  $ZrO_2/Lig$  materials confirming the existence of incorporated lignin. The values obtained for sulfur and carbon may suggest that in both hybrid materials, it contains similar amounts of lignin. EDS mapping results confirm a uniform of Ga, Zr, S, O, and C elements. The data also reveals the presence of slight amount of sodium and iodine in hybrid  $Ga_2O_3/Lig$  and  $ZrO_2/Lig$  materials, which may come from the activation of lignin with sodium periodate. The percentage content of elements was collected and summarized in Table 1.



**Figure 5.** Cont.

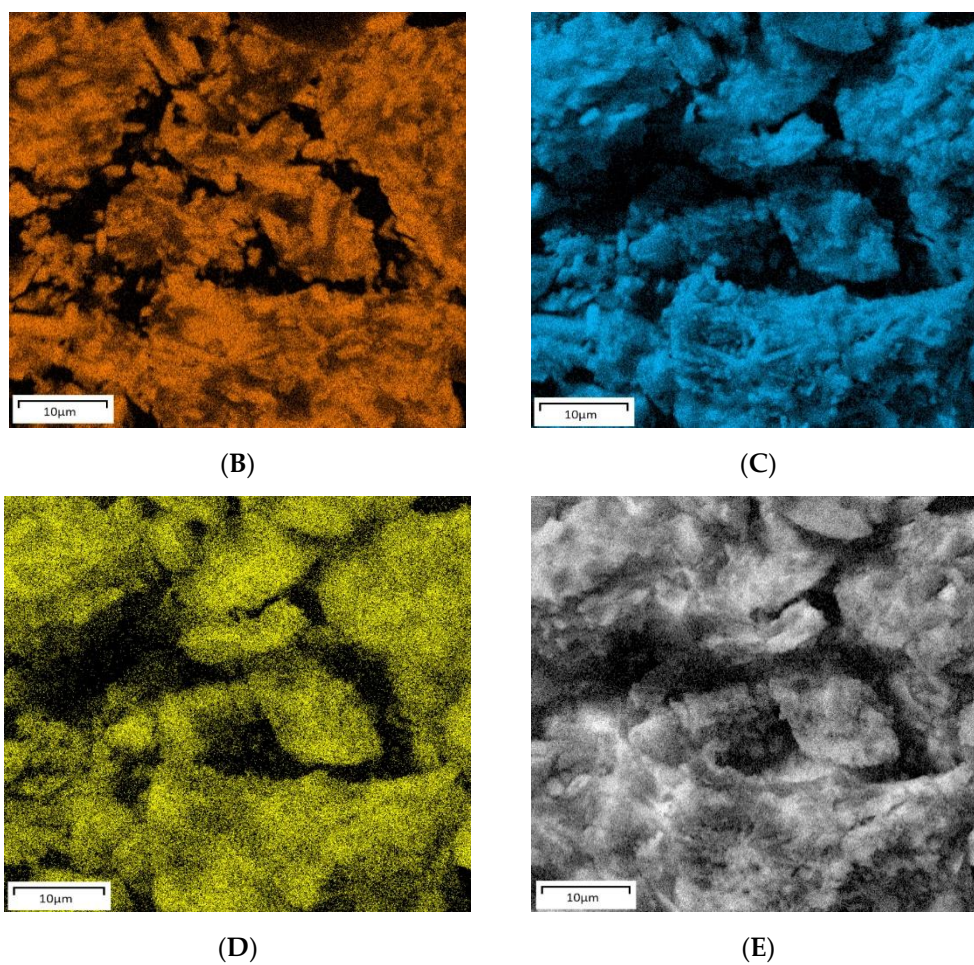
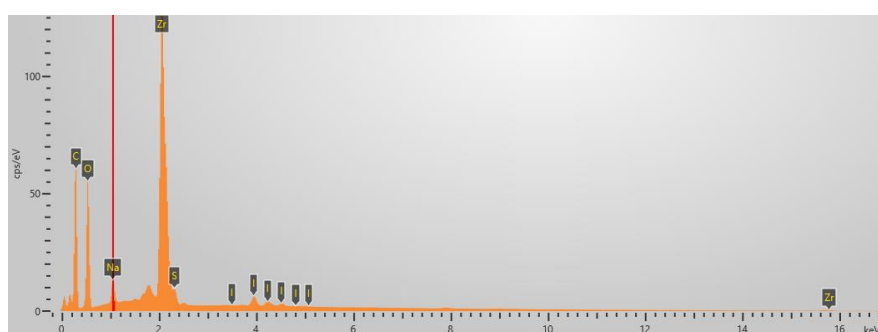


**Figure 5.** EDS mapping spectrum of Ga<sub>2</sub>O<sub>3</sub>/Lig (A) and SEM-micrographs of elemental gallium (B), oxygen (C), sulfur (D), carbon (E).

**Table 1.** EDS analysis results.

Sample	Content of Elements by Weight (%)						
	Ga	Zr	O	C	S	Na	I
Ga <sub>2</sub> O <sub>3</sub>	72.9	-	27.1	-	-	-	-
ZrO <sub>2</sub>	-	67.6	32.4	-	-	-	-
Ga <sub>2</sub> O <sub>3</sub> /Lig	29.0	-	22.3	46.8	0.7	0.4	0.7
ZrO <sub>2</sub> /Lig	-	27.3	25.5	42.9	0.7	1.3	0.7



(A)

**Figure 6.** Cont.

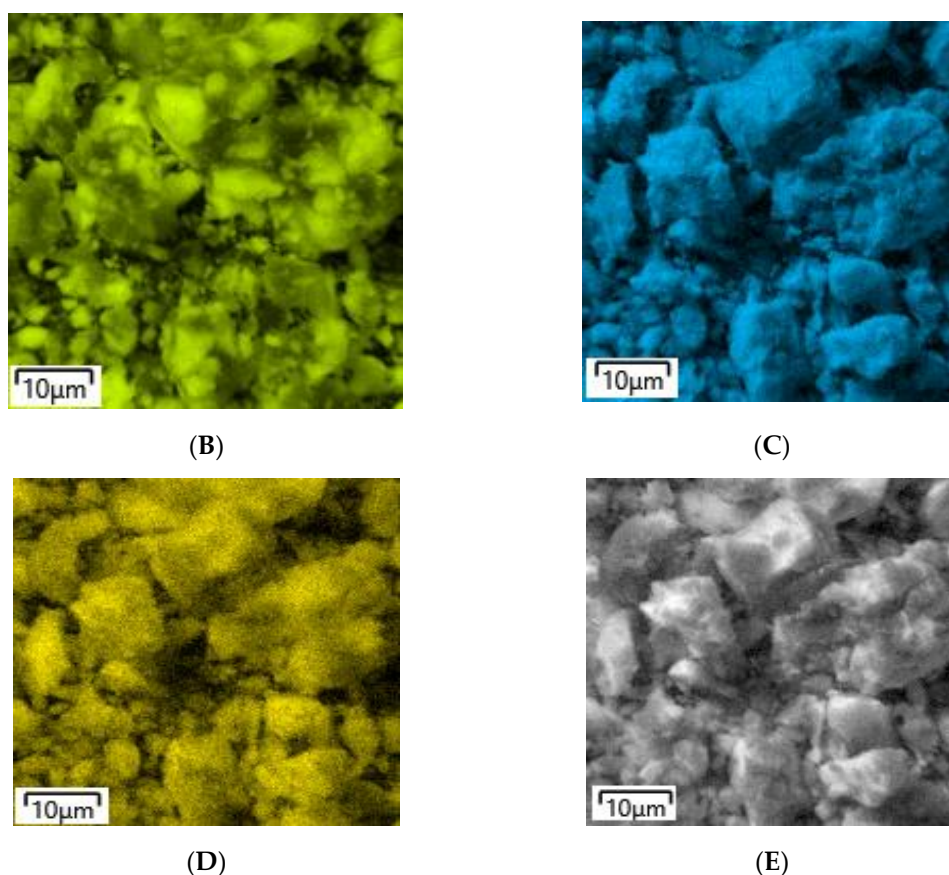


**Figure 6.** EDS mapping spectrum of ZnO<sub>2</sub>/Lig (A) and SEM-micrographs of elemental zirconium (B), oxygen (C), sulfur (D), carbon (E).

In order to determine the crystal structure, an X-ray diffraction analysis for oxides, hybrid materials, and lignin was performed. The XRD patterns are shown in Figure 7. The XRD patterns of Ga<sub>2</sub>O<sub>3</sub> show characteristic peaks at  $2\theta$  values of  $31.72^\circ$ ,  $35.22^\circ$ , and  $63.89^\circ$  correspond to the (002), (111), and (512) diffraction peaks, respectively. All obtained XRD patterns are in accordance with those of monoclinic phase of  $\beta$ -Ga<sub>2</sub>O<sub>3</sub> (JCPDS: 41-1103) [39]. Sharp diffraction peaks also indicate the high crystalline quality of the used compounds. The crystalline structures of ZrO<sub>2</sub> were also investigated with this analysis. The peaks at  $2\theta$  of  $28.74^\circ$ ,  $31.38^\circ$ ,  $50.39^\circ$ , and  $60.47^\circ$  correspond to the (111), (200), (220), and (311) diffraction planes, respectively (JCPDS: 79-1771) [40]. The same diffraction reflections from both oxides and hybrid materials are observed. No Bragg peaks have been noticed in the case of lignin because of the amorphous nature of lignin [41]. The study confirmed that the proposed method of synthesis does not affect the crystal structure of the created materials.

## 2.2. Zeta Potential, Mean Hydrodynamic Diameter, Pdl, and Elemental Analysis of Microplatforms

The Ga<sub>2</sub>O<sub>3</sub>/lignin and ZrO<sub>2</sub>/lignin supports and their components were exposed to electrokinetic potential measurements to define the dispersion stability of individual supports. The results are shown in Table 1. The potential of the metal oxides changed after modification with APTES from  $-32.2$  to  $-28.2$  mV for Ga<sub>2</sub>O<sub>3</sub> and from  $-33.5$  to  $-29.4$  mV for ZrO<sub>2</sub>, respectively. The results indicate the moderate dispersion stability of Ga<sub>2</sub>O<sub>3</sub>/lignin and ZrO<sub>2</sub>/lignin, for which the electrokinetic potential values are  $-35.8$  and  $-36.1$  mV, respectively. The zeta potential of lignin indicates that the biopolymer is very stable [42]. Moreover, the changes in the zeta potentials of these hybrid platforms provide further confirmation of the binding of lignin to the metal oxide surfaces. Furthermore, there were presented sizes of particles based on non-invasive back scattering (NIBS) measurements and the polydispersity index (Pdl) findings of the metal oxides (Ga<sub>2</sub>O<sub>3</sub>, ZrO<sub>2</sub>), before and after APTES-modification and

final hybrid products. The modification of the metal oxides and binding them to the lignin facilitate aggregations and agglomerations of the molecules. The PdI index also increased after both the modification and the hybrid materials synthesis (see Table 2).

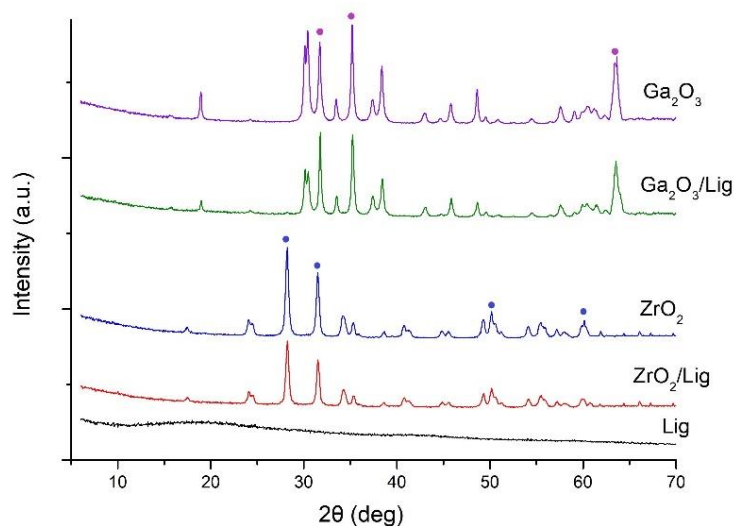


**Figure 7.** XRD patterns of raw  $\text{Ga}_2\text{O}_3$ ,  $\text{ZrO}_2$ , lignin, and  $\text{Ga}_2\text{O}_3/\text{Lig}$ ,  $\text{ZrO}_2/\text{Lig}$  hybrid materials.

**Table 2.** Zeta potential, mean particle size, and polydispersity character of studied samples.

Sample	Zeta Potential (mV)	Mean Hydrodynamic Diameter (nm)	PdI
$\text{Ga}_2\text{O}_3$	−32.2	930–1472	0.35
$\text{ZrO}_2$	−33.5	269–283	0.29
$\text{Ga}_2\text{O}_3$ (modified)	−28.2	1408–1932	0.41
$\text{ZrO}_2$ (modified)	−29.4	348–380	0.37
Lignin	−42.1	280–348	0.19
$\text{Ga}_2\text{O}_3/\text{lignin}$	−35.8	1566–2251	0.69
$\text{ZrO}_2/\text{lignin}$	−36.1	656–785	0.57

The next test to confirm the chemical composition of synthesized samples was elemental analysis. This analysis allowed the determination of the nitrogen (N), carbon (C), hydrogen (H), and sulfur (S) contents. The presence of nitrogen content in the modified metal oxides after APTES-modification were observed. The obtained results are similar for both hybrid materials ( $\text{Ga}_2\text{O}_3/\text{lignin}$ ;  $\text{ZrO}_2/\text{lignin}$ ). The obtained results were presented in Table 3.

**Table 3.** Elemental analysis of  $\text{Ga}_2\text{O}_3/\text{Lig}$ ,  $\text{ZrO}_2/\text{Lig}$ , and their components.

Sample	Elemental Content (%)			
	N	C	H	S
kraft lignin		50.36 ± 0.13	5.79 ± 0.04	3.15 ± 0.08
kraft lignin (activated) *		52.27 ± 0.15	5.09 ± 0.02	2.77 ± 0.05
$\text{Ga}_2\text{O}_3$				
$\text{ZrO}_2$				
$\text{Ga}_2\text{O}_3$ (modified) **	0.34 ± 0.01	5.82 ± 0.04	0.66 ± 0.01	
$\text{ZrO}_2$ (modified) **	0.32 ± 0.01	5.64 ± 0.03	0.62 ± 0.01	
$\text{Ga}_2\text{O}_3/\text{Lig}$	0.23 ± 0.01	19.97 ± 0.01	2.38 ± 0.02	2.22 ± 0.01
$\text{ZrO}_2/\text{Lig}$	0.22 ± 0.01	19.38 ± 0.04	2.34 ± 0.02	1.09 ± 0.01

\* Lignin activated with sodium periodate ( $\text{NaIO}_4$ ). \*\* metal oxides modified by (3-aminopropyl)triethoxysilane (APTES).

### 2.3. Fourier Transform Infrared Spectroscopy (FT-IR) Analysis

FT-IR spectra are shown in Figure 8A,B. The band of stretching vibrations of  $-OH$  groups lies in the wavenumber range  $3600\text{--}3400\text{ cm}^{-1}$  [5]. In the range  $3000\text{--}2800\text{ cm}^{-1}$ , peaks originating from stretching vibrations of  $-CH$  groups ( $CH_3$  and  $CH_2$ ) are noticeable [5]. The signals in the range  $1600\text{--}1475\text{ cm}^{-1}$  are characteristic for stretching vibrations of  $C_{Ar} = C_{Ar}$  groups originating from the aromatic rings of lignin [5].

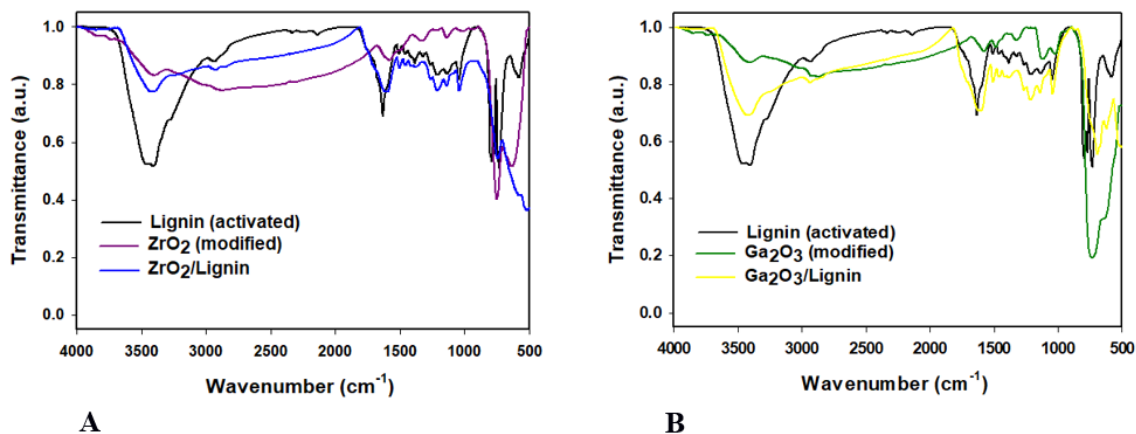


**Figure 8.** FT-IR spectra of lignin, modified Ga<sub>2</sub>O<sub>3</sub> and Ga<sub>2</sub>O<sub>3</sub>/lignin hybrid (A), and lignin, modified ZrO<sub>2</sub> and ZrO<sub>2</sub>/lignin hybrid (B).

Figure 8A shows the FT-IR spectrum of Ga<sub>2</sub>O<sub>3</sub> after modification. As a result of the modification,  $-NH_2$  groups are introduced [43]. The spectrum confirms the effectiveness of the modification due to the presence of a band in the wavenumber range  $3400\text{--}3200\text{ cm}^{-1}$ , derived from stretching vibrations of  $-NH$  bonds [5,43]. The spectrum also includes bands corresponding to the vibrations of functional groups originating from Ga<sub>2</sub>O<sub>3</sub>. The vibrations of Ga–O bonds produce a signal in the wavenumber range  $650\text{--}700\text{ cm}^{-1}$  [43]. Figure 8A also shows the FT-IR spectrum of the Ga<sub>2</sub>O<sub>3</sub>/lignin hybrid. In the range  $3200\text{--}3600\text{ cm}^{-1}$ , increase in the intensity of bands originating from stretching vibrations of  $-OH$  and  $-NH$ , at wavenumber range  $3400\text{--}3200\text{ cm}^{-1}$ , groups are visible, indicating effective obtaining of hybrid [5].

In the spectrum of zirconium dioxide after modification, which is shown in Figure 8B, attention should be paid to the signals in the wavenumber range  $3600\text{--}3400\text{ cm}^{-1}$  generated by stretching vibrations of hydroxyl groups, and the band in the region around  $500\text{ cm}^{-1}$ , characteristic for Zr–O groups [43]. Hydroxyl and amine groups bands increased in intensity following modification with APTES. After binding of the structure of lignin to the metal oxide, bands corresponding to vibrations of C–H bonds are presented at about  $2800\text{ cm}^{-1}$ , and signals in the range  $1500\text{--}1425\text{ cm}^{-1}$  indicate the  $C_{Ar}\text{--}C_{Ar}$  bonds originating from the aromatic structures occurring in the structure of lignin [43].

### 2.4. Thermal Stability

Thermogravimetric analysis (TG) was used to determine the thermal stability of the prepared hybrids (Figure 9).

Measurements were performed in the temperature range up to  $1000\text{ }^\circ\text{C}$ . The TG curves of Ga<sub>2</sub>O<sub>3</sub> before and after modification show insignificant mass loss [44] associated with the loss of water that was connected to the oxide surface with physical bonds. The analysis shows the high thermal stability of Ga<sub>2</sub>O<sub>3</sub> in a wide range of temperatures. From the curve for the Ga<sub>2</sub>O<sub>3</sub>/lignin hybrid system, it can be concluded that the thermal decomposition of the sample consists of three main steps. In the temperature range from  $25\text{ }^\circ\text{C}$  to about  $250\text{ }^\circ\text{C}$ , there is a slight decrease (around 10%) in the mass of the sample, related to the evaporation of water on matrix surface. There is then a rapid decrease in mass by about 30% in a temperature range of approximately  $300\text{--}600\text{ }^\circ\text{C}$  [44]. This is related to the

thermal decomposition of the lignin present in the Ga<sub>2</sub>O<sub>3</sub>/lignin hybrid system. At temperatures above 600 °C, the sample passes along a further loss of mass of about 15%, caused by the thermal degradation of lignin fragments that occur in combination with carbon. Nevertheless, it can be concluded that the Ga<sub>2</sub>O<sub>3</sub>/lignin hybrid system has relatively high thermal stability [4,5,44].

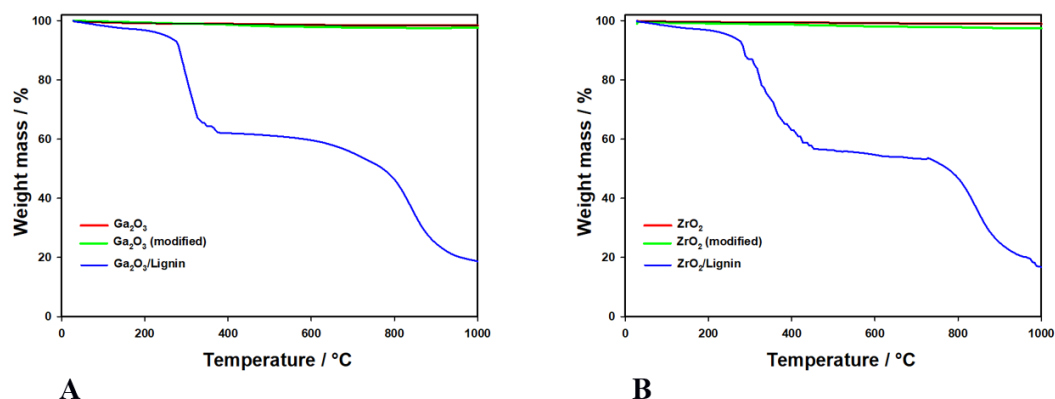


**Figure 9.** TG curves of modified and unmodified Ga<sub>2</sub>O<sub>3</sub> and Ga<sub>2</sub>O<sub>3</sub>/lignin hybrid (A), and modified and unmodified ZrO<sub>2</sub> and ZrO<sub>2</sub>/lignin hybrid (B).

On the graph in Figure 9B, the ZrO<sub>2</sub>/lignin hybrid system is observed to undergo a significant loss of mass of heating compared with unmodified and modified zirconium dioxide. The first mass loss, connected with the elimination of water physically absorbed on the surface of lignin, occurred in the temperature range 25–200 °C and amounted to about 8%. The second larger loss occurred in the range 280–320 °C. This was a loss of about 25%, associated with the loss of crystalline water trapped in the structure of the ZrO<sub>2</sub>/lignin hybrid material [4,5]. Thermal treatment in the third stage above 350 °C (up to 1000 °C) causes a partial loss of lignin fragments associated with carbon decomposition (a mass loss of about 30%), which results from fragmentation of the molecule due to unclear and uncontrolled reactions [3,4].

### 2.5. Efficiency of Glucose Oxidase (GOx) Immobilization

To measure the efficiency of enzyme immobilization, the Bradford method was used. The assay is a spectrophotometric measurement at wavelength  $\lambda = 595$  nm, using a dye called Coomassie Brilliant Blue G-250, which makes a specific combination with amino acid residues containing a positive charge, including mainly arginine, as well as histidine, lysine, proline, tryptophan, and tyrosine. The used G-250 dye links with amino acids that change the colour from brown to blue, which it can be observed at UV-Vis spectrophotometer. The Bradford test is a comparatively universal and effective assay. The adsorption immobilization of GOx on Ga<sub>2</sub>O<sub>3</sub>/lignin or ZrO<sub>2</sub>/lignin hybrid materials was conducted at pH 5.0 and involved the formation of hydrogen bonds between amine groups in the enzyme and the carbonyl groups present in lignin. Studies of the quantity of immobilized GOx was performed using supernatants from presented hybrid materials after immobilization and unbound enzyme. The results are shown in Figure 10.

It may be observed from Figure 10 that the quantity of enzyme immobilized on the material grows as the process time increases up to 24 h. Extending the duration of the process, such as 72 h or 96 h, does not increase the quantity of enzyme adsorbed on the support. This may be due to the saturation of the surface active sites capable of immobilizing the enzyme. The maximum quantities of immobilized glucose oxidase on the Ga<sub>2</sub>O<sub>3</sub>, ZrO<sub>2</sub>, Ga<sub>2</sub>O<sub>3</sub>/lignin, and ZrO<sub>2</sub>/lignin hybrid materials were obtained after 24 h of the process, and reached 9.7, 11.6, 24.7, and 27.1 mg g<sup>-1</sup>, respectively.

The obtained results were compared with our previously created systems and literature data and are summarized in Table 4.

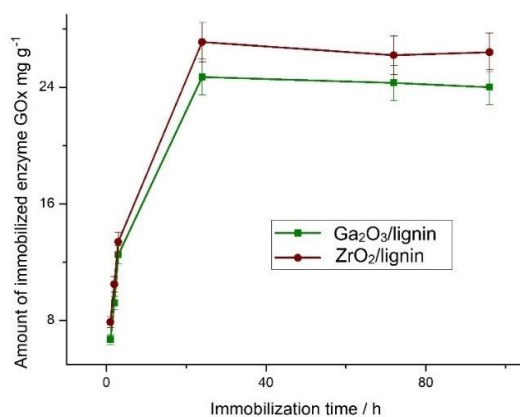


**Figure 10.** Quantity of enzyme immobilized on Ga<sub>2</sub>O<sub>3</sub>/lignin (red line) and ZrO<sub>2</sub>/lignin (green line) from glucose oxidase solution (5 mg mL<sup>-1</sup>) at pH 5, as a function of process duration.

**Table 4.** The amount of GOx immobilized on the different platforms.

Sample	Immobilized GOx/mg g <sup>-1</sup>	Ref.
Silica	12.9	[5]
Graphite	7.6	[5]
SiO <sub>2</sub> /Lig	25.6	[5]
Fe <sub>3</sub> O <sub>4</sub> /Lig/PDA	29.4	[45]
PolymP <sup>®</sup> -Link	12.0	[46]
CaTi <sub>4</sub> (PO <sub>4</sub> ) <sub>6</sub>	27.0	[47]
MIMNs	33.0	[48]
Ga <sub>2</sub> O <sub>3</sub>	9.7	This work
ZrO <sub>2</sub>	11.6	This work
Ga <sub>2</sub> O <sub>3</sub> /Lig	24.7	This work
ZrO <sub>2</sub> /Lig	27.1	This work

To confirm the immobilization of GOx on the surfaces of the hybrids and to examine changes in the surface topography, AFM measurements were carried out (Figure 11).

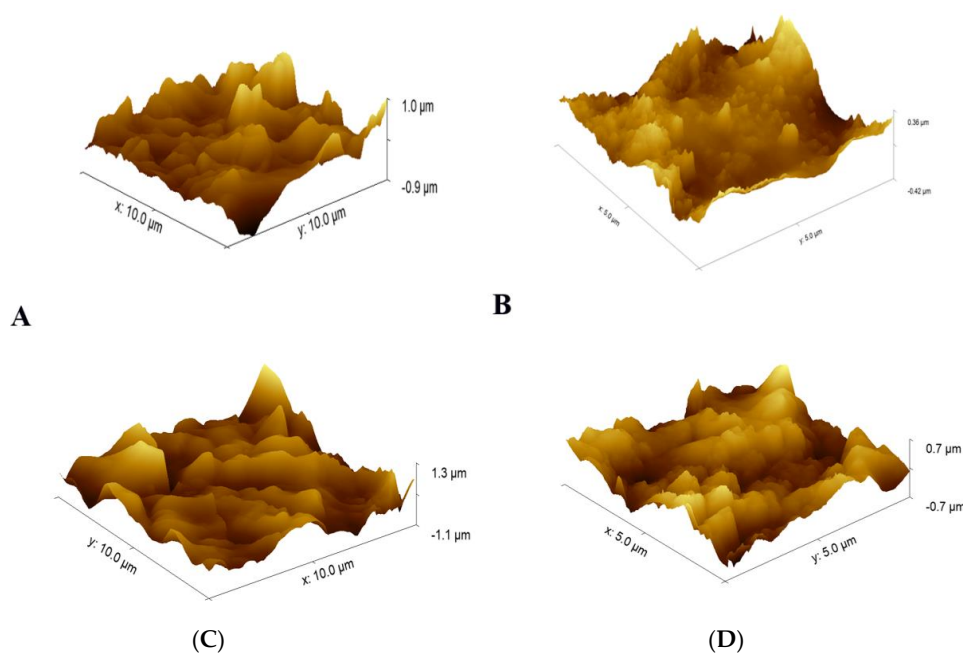
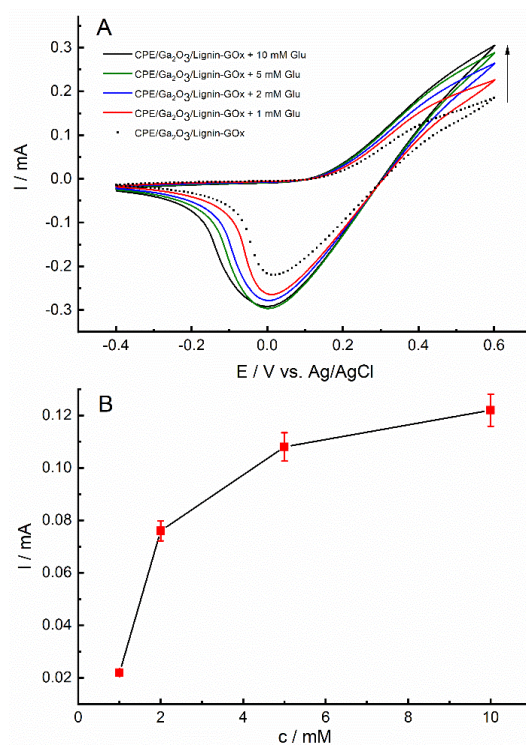


**Figure 11.** AFM images of Ga<sub>2</sub>O<sub>3</sub>/Lig (A), ZrO<sub>2</sub>/Lig (B), Ga<sub>2</sub>O<sub>3</sub>/Lig/GOx (C) and ZrO<sub>2</sub>/Lig/GOx (D).

Variable changes take place in the samples before and after the immobilization process. The parameter  $Z$  on the AFM images increases for the systems containing enzyme. In addition, the surface structure of the matrix becomes rougher, which may suggest that the surface is covered with objects of a larger size in relation to the native roughness of the lignin.

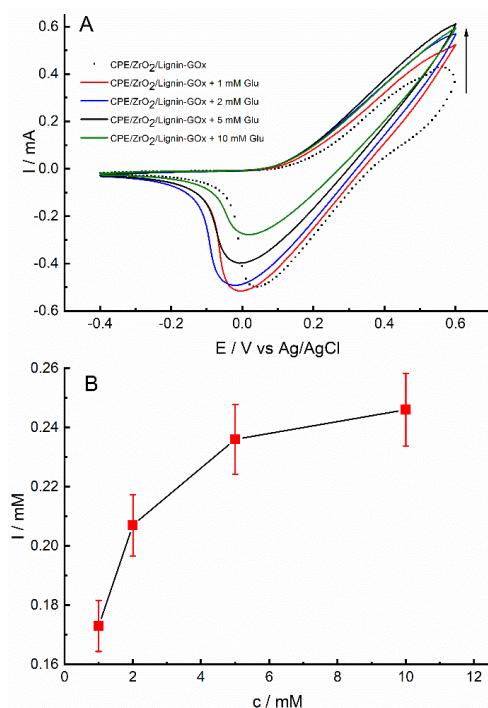
### 2.6. Electrochemical Properties of Electrocatalytic Microplatforms with Immobilized Glucose Oxidase

Figure 12A shows cyclic voltammograms of CPE/Ga<sub>2</sub>O<sub>3</sub>/lignin-GOx in PBS in the absence of glucose and in the presence of 1, 2, 5, and 10 mM glucose. Ferrocene mediator was incorporated into the electrode to provide electrochemical communication between GOx active sites and the electrode surface. It can be seen that the oxidation was accomplished based on a clear increase in the anodic current at a potential close to the formal potential for ferrocene. This behavior indicates that the CPE/Ga<sub>2</sub>O<sub>3</sub>/lignin-GOx electrode is able to catalyze the oxidation of glucose using Fc<sup>+</sup>/Fc as an effective mediator. As shown by the plot in Figure 11B, the anodic current increased with increasing glucose concentration. All electrochemical tests were repeated three times and were characterized by high repeatability.



**Figure 12.** Cyclic voltammograms of CPE/Ga<sub>2</sub>O<sub>3</sub>/lignin-GOx recorded in PBS (pH 7.4) in the absence of glucose and in the presence of different glucose concentrations (A). Scan rate 10 mV s<sup>-1</sup>. Oxidative current dependence on glucose concentration (B).

Similar results were obtained for the CPE/ZrO<sub>2</sub>/lignin-GOx modified electrode system (Figure 13). It is observed that the higher the glucose concentration, the higher the anodic current recorded at the CPE/ZrO<sub>2</sub>/lignin-GOx. Moreover, the shape of the  $I$  vs.  $c$  curve in Figure 13B suggests that the enzymatic reaction follows Michaelis–Menten kinetics [49].



**Figure 13.** Cyclic voltammograms of CPE/ZrO<sub>2</sub>/lignin-GOx recorded in PBS (pH 7.4) in the absence of glucose and in the presence of different glucose concentrations (A). Scan rate 10 mV s<sup>-1</sup>. Plot of oxidation current vs. glucose concentration (B).

### 3. Materials and Methods

#### 3.1. Materials and Chemicals

The components used in this work were gallium oxide (Ga<sub>2</sub>O<sub>3</sub>), zirconium(IV) oxide (ZrO<sub>2</sub>), kraft lignin, phosphate buffer saline (PBS) (pH 7.4; 10 mM), citric buffer (pH 5.0; 10 mM), sodium iodate, methanol, dioxane, APTES, glucose oxidase from *Aspergillus niger*, ferrocene, and glucose solutions (1, 2, 5, and 10 mM). A basic biosensor was constructed using carbon paste electrode (CPE), ferrocene, and graphite. The chemical reagents were purchased from Sigma-Aldrich (St. Louis, MO, USA) with the exception of the CPE (BASi, West Lafayette, IN, USA). Reagents and solvents used in the research were reagent-grade quality.

#### 3.2. Modification of Metal Oxide Materials

To obtain modified oxides (gallium oxide and zirconium (IV) oxide) a solution consisting of (3-aminopropyl) triethoxysilane (APTES):water:methanol in the ratio 1:4:16 was prepared. The modification was carried out using 6 g of one of the oxides and 6.3 mL of the modifying solution (0.3 mL of APTES, 1.2 mL of H<sub>2</sub>O, 4.8 mL of MeOH). The modifying solution was added to the oxide with constant stirring. The final paste product was dried at 105 °C for 24 h. The last stage of the modification consisted in grinding and sieving the obtained modified oxide through a sieve with a mesh size of 64 μm. The mechanism of modification of selected oxides with the APTES is presented in Figure 14.

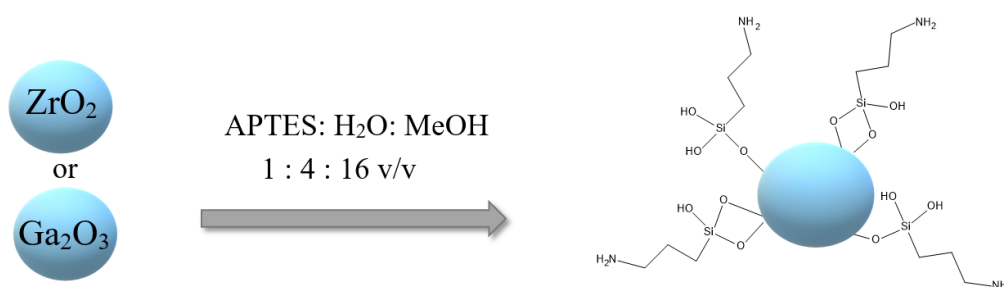


**Figure 14.** Scheme of modification of  $ZrO_2$  and  $Ga_2O_3$ .

### 3.3. Activation of Lignin and Synthesis of $Ga_2O_3$ /Lignin and $ZrO_2$ /Lignin Supports

In a 500 mL glass reactor equipped with a peristaltic pump, 4 g of lignin, 200 mL of dioxane, and 22.5 mL of distilled water were mixed. Next, 6 g of sodium iodate dissolved in 120 mL of water was added at a rate of  $12 \text{ mL min}^{-1}$ . To ensure that the lignin oxidized only under the influence of the oxidant, the reactor was sealed with silver foil. This caused the oxidation process to occur only under the impact of sodium periodate ( $NaIO_4$ ), excluding oxidation under the influence of light. The reaction of chemical activation of lignin lasted 80 min. The mechanism of this synthesis is presented in Figure 15.

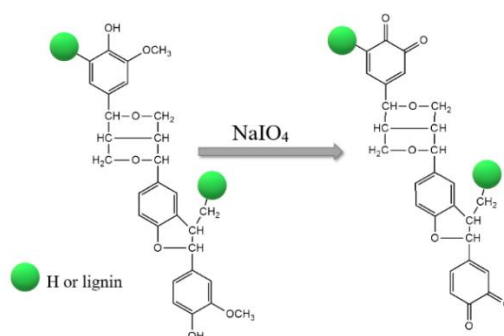


**Figure 15.** Schematic representation of lignin activation.

In the next step, the 4 g of modified oxide ( $Ga_2O_3$  or  $ZrO_2$ ) was added to the reaction mixture. Media synthesis reactions were carried out for 1 h with continuous stirring. The next step was evaporation of the solvents in an evaporator. The obtained dry powder was washed with distilled water and left in an oven at  $105 \text{ }^\circ\text{C}$  for 24 h. This step is schematically shown in Figure 16.

### 3.4. Immobilization of Glucose Oxidase on $Ga_2O_3$ /Lignin and $ZrO_2$ /Lignin Supports

Before the adsorption immobilization process, an enzyme solution was prepared in a  $10 \text{ mg mL}^{-1}$  PBS phosphate saline buffer. Next, 50 mg of the support and 20 mL of the previously prepared solution of glucose oxidase were combined. The reaction system was stirred using a magnetic stirrer for 1, 2, 3, 24, 72, or 96 h. Immobilization was carried out at ambient temperature. After the immobilization process was completed, the solution was poured out and centrifuged for 15 min at 15,000 rpm. The resulting filtrate was then separated and the precipitate was dried at ambient temperature for 24 h. Furthermore, the Bradford method was a technique that could not be used to determine the efficiency of immobilization for kraft lignin as a component. As presented in previous works, the kraft lignin is well-soluble in water, which made it impossible to use the Bradford method [50]. Figure 17 shows a schematic process of glucose oxidase immobilization on the  $Ga_2O_3$ /lignin and  $ZrO_2$ /lignin matrix surfaces.

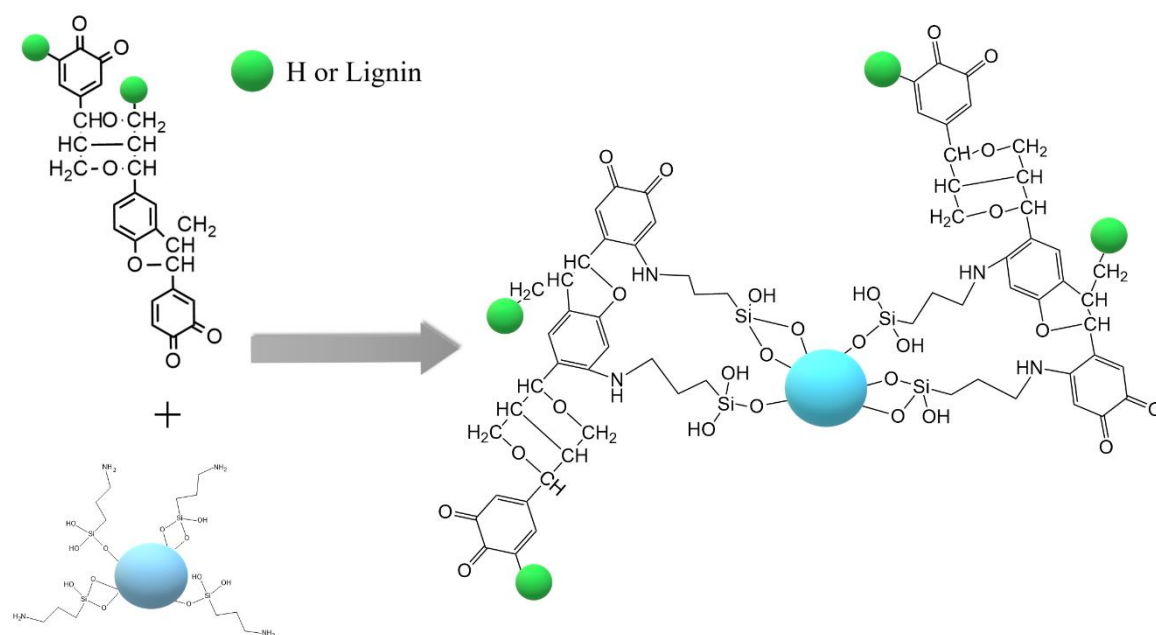


**Figure 16.** Diagram showing the creation of  $ZrO_2/Lig$  and  $Ga_2O_3/Lig$  hybrid materials.

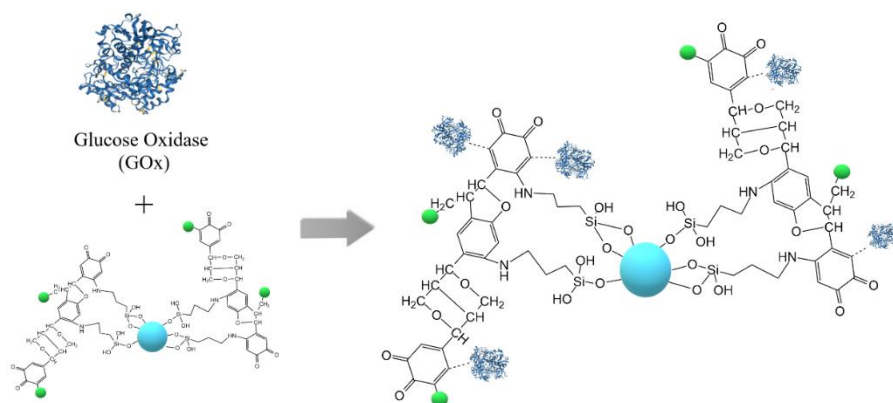


**Figure 17.** Schematic representation of glucose oxidase immobilization on the synthesized materials.

The mechanism by which enzyme binds to lignin has been presented previously in the literature [50,51]. These studies have shown that the activity of the immobilized enzyme on the matrix surface slightly decreases, which is determined by the formation of hydrogen bonds and ionic interactions between the enzyme and matrix [51,52].

### 3.5. Construction of an Enzymatic Biosensor

To construct an enzyme biosensor, a paste composed of 15 mg of  $Ga_2O_3/lignin/GOx$  or  $ZrO_2/lignin/GOx$ , 15 mg of graphite and 2 mg of ferrocene mediator was hand-mixed in a mortar, with one drop of paraffin oil used as a binder. Freshly made paste was used to construct the carbon paste electrode, as shown in Figure 18.

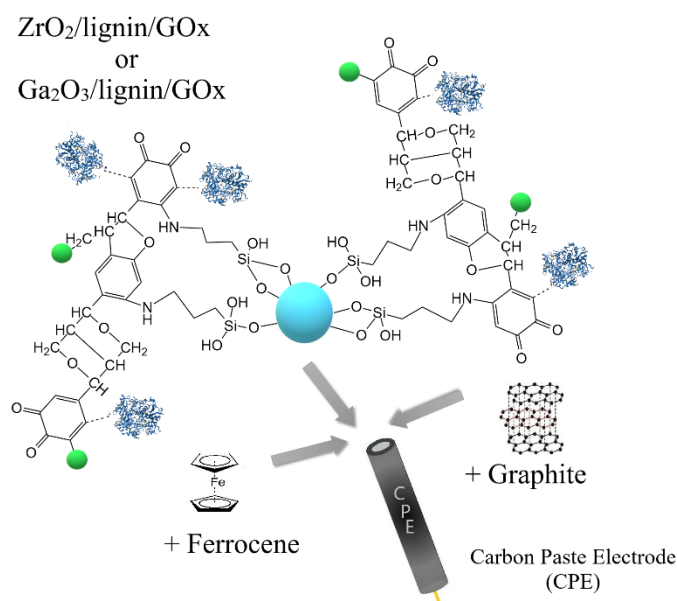


**Figure 18.** Biosensor construction based on  $Ga_2O_3$ /lignin/GOx or  $ZrO_2$ /lignin/GOx material.

### 3.6. Physicochemical Analysis

To determine the functional groups present in the structure of the hybrid materials, they were subjected to Fourier transform infrared spectroscopy (FT-IR). FT-IR spectra were collected using a Vertex 70 spectrometer (Bruker, Billerica, MA, USA). Materials for analysis were tested in the form of tablets, previously prepared by mixing 2 mg of the test substance and 250 mg of anhydrous KBr at a pressure of 10 MPa. The FT-IR analyses were performed at a resolution of  $0.5\text{ cm}^{-1}$  in the wavenumber range of  $4000\text{--}500\text{ cm}^{-1}$ . TEM analysis records the electrons passing through the sample. A Jeol analyzer (JEM-1400) was used for the analysis, with 120 kV maximum acceleration and 2 nm resolution. Atomic Force Microscopy was performed using an Agilent 5500 atomic force microscope in intermittent contact mode in ambient conditions. The test material from the solution was applied to the surface of mica, which was earlier cleaned by mechanical removal of stripping. The test material was applied to the substrate by spin coating. An Allin One cantilever (BudgetSensors, Sofia, Bulgaria) with a resonance frequency of approximately 150 kHz was used for scanning. The surface morphology of the samples were determined using scanning electron microscope with energy dispersive spectroscopy (SEM-EDS). The tests were performed on a Jeol 7001TTLS (Jeol SAS, Croissy, France) with 30 kV maximum acceleration and 1.5 nm resolution. To assess the stability of materials in liquid solvent, zeta potential (ZP) analysis was performed using a Zetasizer Nano ZS (Malvern Instruments Ltd., Malvern, UK) with a range of 0.6–6000 nm. Thermogravimetric analysis (TGA) was carried out using a Jupiter STA 449 F3 instrument (Netzsch, Selb, Germany). The XRD analysis was made using a D8 Advance X-ray diffractometer (Bruker, Billerica, MA, USA). The elemental analysis was made using a Vario EL Cube apparatus (Elementar Analysensysteme GmbH, Langenselbold, Germany). A 10 mg of sample was used for analysis. During the process, a sample was combusted in an oxygen atmosphere, and after that, transferred onto the reduction column. The resulting gases were separated in an adsorption column, and then recorded using a detector. The results are given as averages of three measurements, each accurate to 0.0001%.

### 3.7. Electrochemical Study

Electrochemical tests were carried out in a three-electrode system using an Autolab (PGSTAT-30) electrochemical analyzer (Eco Chemie, Utrecht, Netherlands). A carbon paste electrode (BASi, West Lafayette, IN, USA) was used for the working electrodes (CPE/ $Ga_2O_3$ /lignin/GOx/Fc and CPE/ $ZrO_2$ /lignin/GOx/Fc). Silver chloride electrode Ag/AgCl (3 M KCl) was the reference electrode and

platinum wire the counter electrode. All electrochemical tests were conducted in ambient temperature in at phosphate buffer pH 7.4.

#### 4. Conclusions

In this paper, we have presented attractive alternative microplatforms for enzyme immobilization and biosensing. The support obtained exhibited good affinity for the immobilization of glucose oxidase (GOx). A higher amount of the GOx ( $27.1 \text{ mg g}^{-1}$ ) was immobilized on  $\text{ZrO}_2/\text{lignin}$  carrier than on  $\text{Ga}_2\text{O}_3/\text{lignin}$  ( $24.7 \text{ mg g}^{-1}$ ). The  $\text{Ga}_2\text{O}_3/\text{lignin-GOx}$  and  $\text{ZrO}_2/\text{lignin-GOx}$  systems, with ferrocene and carbon paste (BASi), exhibited satisfied electrochemical properties in the catalytic oxidation of glucose. The microplatforms are suitable materials for the preparation of efficient and cheap supports for biocatalysts and for biosensor application.

A review of the literature indicates the higher interest of research on metal oxides and the development of microcarriers for industrial and environmental applications indeed. An interesting application may be the use of an enzyme biosensor for glucose detection based on the aforementioned micromaterials, as produced in this study.

**Author Contributions:** Methodology and planning of studies (A.J., T.R., T.J.); Synthesis and preparation of the hybrids (A.J.; M.K.); Evaluation of enzyme immobilization efficiency and stability (A.J.; J.Z.); Electrochemical support (T.R.), preparation of the manuscript (A.J.; M.K.; T.R.), Elemental analysis study (A.K.-R.), description part of the manuscript (A.K.-R., J.Z., A.P.), Energy-dispersive X-ray spectroscopy analysis (A.P.), Coordination of all research tasks and evaluation of the manuscript (T.J.).

**Funding:** This work was founded by the National Science Center Poland, no. 2017/27/B/ST8/01506.

**Acknowledgments:** The authors are grateful to Monika Gwizdała and Karolina Hały for substantive support.

**Conflicts of Interest:** The authors declare no conflict of interest.

#### References

1. Nanko, M. Definitions and categories of hybrid materials. *AZojomo* **2009**, *6*, 1–8.
2. Chung, D.D.L. *Composite Materials, Kirk-Othmer Encyclopedia of Chemical Technology*; Wiley-VCH: New York, NY, USA, 2011.
3. Jesionowski, T.; Klapiszewski, Ł.; Milczarek, G. Structural and electrochemical properties of multifunctional silica/lignin materials. *Mat. Chem. Phys.* **2014**, *147*, 1049–1057. [[CrossRef](#)]
4. Klapiszewski, Ł.; Nowacka, M.; Milczarek, G.; Jesionowski, T. Physicochemical and electrokinetic properties of silica/lignin biocomposites. *Carbohydr. Polym.* **2013**, *94*, 345–355. [[CrossRef](#)] [[PubMed](#)]
5. Jędrzak, A.; Rebiś, T.; Klapiszewski, Ł.; Zdarta, J.; Milczarek, G.; Jesionowski, T. Carbon paste electrode based on functional GOx/silica-lignin system to prepare an amperometric glucose biosensor. *Sens. Actuators B* **2018**, *256*, 176–185. [[CrossRef](#)]
6. KICKELBICK, G. *Hybrid Materials: Synthesis, Characterization and Applications*; John Wiley & Sons: Wien, Austria, 2007.
7. Gomez-Romero, P.; Sanchez, C. *Functional Hybrid Materials*; John Wiley & Sons: Darmstadt, Germany, 2006.
8. Kango, S.; Kalia, S.; Celli, A.; Njuguna, J.; Habibi, Y.; Kumar, R. Surface modification of inorganic nanoparticles for development of organic–inorganic nanocomposites—A review. *Prog. Polym. Sci.* **2013**, *38*, 1232–1261. [[CrossRef](#)]
9. Drisko, D.L.; Sanchez, C. Hybridization in Materials Science—Evolution, Current State, and Future Aspirations. *Eur. J. Inorg. Chem.* **2012**, *32*, 5097–5105. [[CrossRef](#)]
10. Yoon, K.; Takahashi, S.; Nge, T.T.; Nakagawa-izumi, A.; Ohi, H.; Yamada, T. Characterization of lignin derivatives in alkaline polyethylene glycol-treated soda cooking black liquor powder. *BioResources* **2016**, *3*, 6426–6437. [[CrossRef](#)]
11. Bajwa, D.S.; Wang, X.; Sitz, E.; Loll, T.; Bhattacharje, S. Application of bioethanol derived lignin for improving physico-mechanical properties of thermoset biocomposites. *Int. J. Biol. Macromol.* **2016**, *89*, 265–272. [[CrossRef](#)]

12. Espinoza-Acosta, J.L.; Torres-Chávez, P.I.; Ramírez-Wong, B.; López-Saiz, C.M.; Montaña-Leyva, B. Antioxidant, antimicrobial, and antimutagenic properties of technical lignins and their applications. *BioResources* **2016**, *11*, 5452–5481. [[CrossRef](#)]
13. Jesionowski, T.; Zdarta, J.; Krajewska, B. Enzyme immobilization by adsorption: A review. *Adsorption* **2014**, *20*, 801–821. [[CrossRef](#)]
14. Zdarta, J.; Meyer, A.S.; Jesionowski, T.; Pinelo, M. Developments in support materials for immobilization of oxidoreductases: A comprehensive review. *Adv. Colloids Interf.* **2018**, *258*, 1–20. [[CrossRef](#)] [[PubMed](#)]
15. Mohamad, N.; Marzuki, N.; Buang, N.; Huyop, F.; Wahab, R. An overview of technologies for immobilization of enzymes and surface analysis techniques for immobilized enzymes. *Biotechnol. Equip.* **2015**, *29*, 205–220. [[CrossRef](#)] [[PubMed](#)]
16. Zdarta, J.; Klapiszewski, Ł.; Jędrzak, A.; Nowicki, M.; Moszynski, D.; Jesionowski, T. Lipase B from *Candida antarctica* Immobilized on a Silica-Lignin Matrix as a Stable and Reusable Biocatalytic System. *Catalysts* **2017**, *7*, 14. [[CrossRef](#)]
17. Zdarta, J.; Jędrzak, A.; Klapiszewski, Ł.; Jesionowski, T. Immobilization of Cellulase on a Functional Inorganic–Organic Hybrid Support: Stability and Kinetic Study. *Catalysts* **2017**, *7*, 374. [[CrossRef](#)]
18. Bankar, S.B.; Bule, M.V.; Singhal, R.S.; Ananthanarayan, L. Glucose oxidase—An overview. *Biotechnol. Adv.* **2009**, *27*, 489–501. [[CrossRef](#)] [[PubMed](#)]
19. Batule, B.S.; Park, K.S.; Gautam, S.; Cheon, H.J.; Kim, M.I.; Park, H.G. Intrinsic peroxidase-like activity of sonochemically synthesized protein copper nanoflowers and its application for the sensitive detection of glucose. *Sens. Actuator B-Chem.* **2018**, *283*, 749–754. [[CrossRef](#)]
20. Baghayeri, M.; Veisi, H.; Ghanei-Motlagh, M. Amperometric glucose biosensor based on immobilization of glucose oxidase on a magnetic glassy carbon electrode modified with a novel magnetic nanocomposite. *Sens. Actuator B-Chem.* **2017**, *249*, 321–330. [[CrossRef](#)]
21. Wong, C.M.; Wong, K.H.; Chen, X.D. Glucose oxidase: Natural occurrence, function, properties and industrial applications. *Appl. Microbiol. Biotechnol.* **2008**, *78*, 927–938. [[CrossRef](#)]
22. Wang, J. Nanomaterial-based electrochemical biosensors. *Analyst* **2005**, *130*, 421–426. [[CrossRef](#)]
23. Valentini, F.; Palleschi, G. Nanomaterials and analytical chemistry. *Anal. Lett.* **2008**, *41*, 479–520. [[CrossRef](#)]
24. Wang, D.; Lou, Y.; Wang, R.; Wang, P.; Zheng, X.; Zhang, Y.; Jiang, N. Humidity sensor based on Ga<sub>2</sub>O<sub>3</sub> nanorods doped with Na<sup>+</sup> and K<sup>+</sup> from GaN powder. *Ceramics Int.* **2015**, *41*, 14790–14797. [[CrossRef](#)]
25. Nikolaev, V.I.; Maslov, V.; Stepanov, S.I.; Pechnikov, A.I.; Krymov, V.; Nikitinac, I.P.; Guzilova, L.I.; Bougrov, V.E.; Romanov, A.E. Growth and characterization of beta-Ga<sub>2</sub>O<sub>3</sub> crystals. *J. Crystal Growth* **2016**, *457*, 132–136. [[CrossRef](#)]
26. Ramana, C.V.; Rubio, E.J.; Barraza, C.D.; Gallardo, A.M.; Mcpeak, S. Chemical bonding, optical constants, and electrical resistivity of sputter-deposited gallium oxide thin films. *J. Appl. Phys.* **2014**, *115*, 1–10. [[CrossRef](#)]
27. Ai, M.; Guo, D.; Qu, Y.; Cui, W.; Wu, Z.; Li, P.; Li, L.; Tang, W. Fast-response solar-blind ultraviolet photodetector with a graphene/β-Ga<sub>2</sub>O<sub>3</sub>/graphene hybrid structure. *J. Alloy. Compd.* **2016**, *692*, 634–638. [[CrossRef](#)]
28. Jung, J.; Cho, W.; Kim, J.; Hwang, K.; Kang, E.; Han, K. Morphological and crystal structural characterization of Ga<sub>2</sub>O<sub>3</sub> particles synthesized by a controlled precipitation and polymerized complex method. *Ceram. Int.* **2016**, *42*, 2582–2588. [[CrossRef](#)]
29. Jena, K.; Narayan, R.; Raju, K. Surface functionalized zinc oxide (ZnO) nanoparticle filled organic–inorganic hybrid materials with enhanced thermo-mechanical properties. *Prog. Org. Coat.* **2015**, *89*, 82–90. [[CrossRef](#)]
30. Siddiqui, M.R.H.; Al-Wassil, A.I.; Al-Otaibi, A.M.; Mahfouz, R.M. Effects of Precursor on the Morphology and Size of ZrO<sub>2</sub> Nanoparticles, Synthesized by Sol-gel Method in Non-aqueous Medium. *Mater. Res.* **2012**, *15*, 986–989. [[CrossRef](#)]
31. Deshmane, V.G.; Adewuyi, Y.G. Synthesis of thermally stable, high surface area, nanocrystalline mesoporous tetragonal zirconium dioxide (ZrO<sub>2</sub>): Effects of different process parameters. *Micropor. Mesopor. Mat.* **2012**, *148*, 88–100. [[CrossRef](#)]
32. Jayakumar, S.; Ananthapadmanabhan, P.V.; Perumal, K. Characterization of nano-crystalline ZrO<sub>2</sub> synthesized via reactive plasma processing. *Mater. Sci. Eng. B* **2011**, *176*, 894–899. [[CrossRef](#)]
33. Mallakpour, S.; Dinari, M.; Neamani, S. Surface Treatment of ZrO<sub>2</sub> Nanoparticles with Biosafe Citric Acid and Its Utilization for the Synthesis of L-Leucine Based Poly(amide-imide) Nanocomposites. *Polym. Plast. Technol. Eng.* **2015**, *54*, 1634–1643. [[CrossRef](#)]

34. Sidhu, G.K.; Kaushik, A.K.; Rana, S.; Bhansali, S. Photoluminescence quenching of Zirconia nanoparticle by surface modification. *Appl. Surf. Sci.* **2015**, *334*, 216–221. [[CrossRef](#)]
35. Wang, J.; Sun, X.; Wei, A. Zinc oxide nanocomb biosensor for glucose detection. *Appl. Phys. Lett.* **2006**, *88*, 233106. [[CrossRef](#)]
36. Marie, M.; Mandal, S.; Manasreh, O. An electrochemical glucose sensor based on zinc oxide nanorods. *Sensors* **2015**, *15*, 18714–18723. [[CrossRef](#)] [[PubMed](#)]
37. Patil, D.; Jung, H.; Dung, N. Enzymatic glucose biosensor based on CeO<sub>2</sub> nanorods synthesized by non-isothermal precipitation. *Biosens. Bioelectron.* **2012**, *31*, 176–181. [[CrossRef](#)]
38. Golikova, E.; Lakina, N.; Grebennikova, O.; Matveeva, V.; Sulman, E. A study of biocatalysts based on glucose oxidase. *Faraday Discuss.* **2017**, *202*, 303–314. [[CrossRef](#)]
39. Wang, Y.; Li, N.; Duan, P.; Sun, X.; Chu, B.; He, Q.; He, Q. Properties and Photocatalytic Activity of  $\beta$ -Ga<sub>2</sub>O<sub>3</sub> Nanorods under Simulated Solar Irradiation. *J. Nanomater.* **2015**, *16*, 1–5.
40. Sathyaseelan, B.; Elayaperumal, M.; Baskaran, I.; Senthilnathan, K.; Sivakumar, K.; Moodley, M.; Ladchumananandasivam, R.; Maaza, M. Studies on structural and optical properties of ZrO<sub>2</sub> nanopowder for opto-electronic applications. *J. Alloy. Compd.* **2017**, *694*, 556–559. [[CrossRef](#)]
41. Goudarzi, A.; Lin, L.T.; Ko, F.K. X-ray diffraction analysis of kraft lignins and lignin-derived carbon nanofibers. *J. Nanotechnol. Eng. Med.* **2014**, *5*, 021006. [[CrossRef](#)]
42. Luxbacher, T. *The Zeta Guide: Principles of the Streaming Potential Technique*; Anton Paar GmbH: Graz, Austria, 2014.
43. Silverstein, R.M.; Webster, F.; Kiemle, D. *Spectrophotometric Identification of Organic Compounds*; John Wiley and Sons: New York, NY, USA, 2005.
44. Reddy, L.S.; Ko, Y.H.; Yu, J.S. Hydrothermal Synthesis and Photocatalytic Property of  $\beta$ -Ga<sub>2</sub>O<sub>3</sub> Nanorods. *Nanoscale Res. Lett.* **2015**, *10*, 1–7. [[CrossRef](#)]
45. Jędrzak, A.; Rębiś, T.; Kuznowicz, M.; Jesionowski, T. Bio-inspired magnetite/lignin/polydopamine-glucose oxidase biosensing nanoplatform. From synthesis, via sensing assays to comparison with others glucose testing techniques. *Int. J. Biol. Macromol.* **2019**, *127*, 677–682. [[CrossRef](#)]
46. Ramon-Marquez, T.; Medina-Castillo, A.L.; Fernandez-Sanchez, J.F.; Fernandez-Gutiérrez, A. Evaluation of different functional groups for covalent immobilization of enzymes in the development of biosensors with oxygen optical transduction. *Anal. Methods* **2015**, *7*, 2943–2949. [[CrossRef](#)]
47. Mohammad, R.; Mojtaba, A. Immobilization of glucose oxidase on meso-porous glassceramic with the skeleton of CaTi<sub>4</sub>(PO<sub>4</sub>)<sub>6</sub>. *J. Adv. Mater. Process.* **2013**, *2*, 57–65.
48. Abbasi, M.; Amiri, R.; Bordbar, A.K.; Ranjibakhsh, E.; Khosropour, A.R. Improvement of the Stability and Activity of Immobilized Glucose Oxidase on Modified Iron Oxide Magnetic Nanoparticles. *Appl. Surf. Sci.* **2016**, *364*, 752–757. [[CrossRef](#)]
49. Berg, J.M.; Tymoczko, J.L.; Stryer, L. *Biochemistry*; W. H. Freeman: New York, NY, USA, 2002.
50. Bradford, M.M. A rapid and sensitive method for the quantitation microgram quantities of protein utilizing the principle of protein-dye binding. *Anal. Biochem.* **1976**, *254*, 248–254. [[CrossRef](#)]
51. Klapiszewski, L.; Zdarta, J.; Jesionowski, T. Titania/lignin hybrid materials as a novel support for  $\alpha$ -amylase immobilization: A comprehensive study. *Colloids Surf. B Biointerfaces* **2018**, *162*, 90–97. [[CrossRef](#)] [[PubMed](#)]
52. Khan, M.J.; Khan, F.H.; Husain, Q.N. Application of Immobilized Ipomoea batata  $\beta$  Amylase in the Saccharification of Starch. *J. Appl. Biol. Sci.* **2011**, *5*, 33.

